A physics-based constitutive model for machining simulation of Ti-6Al-4V titanium alloy

Available online at www.sciencedirect.com

ScienceDirect

Procedia CIRP 117 (2023) 335–340

www.elsevier.com/locate/procedia

19th CIRP Conference on Modeling of Machining Operations

A physics-based constitutive model for machining simulation of Ti-6Al-4V titanium alloy

Amir Malakizadi[a,*], Jannis Saelzer[b], Sebastian Berger[b], Youssef Alammari[b], Dirk Biermann[b]

[a] *Department of Industrial and Materials Science, Chalmers University of Technology, SE-412 96, Gothenburg, Sweden*
[b] *Institute of Machining Technology, TU Dortmund University, Baroper Str. 303, 44227 Dortmund, Germany*

* Corresponding author. Tel.: +46-31-772 63 77; fax: +46 (0)31 772 34 85. *E-mail address:* amir.malakizadi@chalmers.se

Abstract

Today, simulation of cutting processes still relies, in most cases, on the phenomenological representation of flow stress properties of workpiece materials. This investigation presents a physics-based (dislocation-based) constitutive model to simulate the flow stress properties of Ti6Al4V titanium alloy at elevated temperatures and a large range of strain rates. The Split Hopkinson Pressure Bar (SHPB) data and inverse modelling of orthogonal cutting tests are combined using a novel approach to obtain flow stress properties and to calibrate the damage and friction models. The applicability of the presented model for cutting simulation is critically discussed.

Keywords: FEM; Dislocaiton-based; Ti6Al4V; SHPB; Inverse identification

1. Introduction

Over the last decades, Finite Element Method (FEM) has widely been used for modelling and simulation of the machining processes. The main aim is to provide a better understanding of the complex phenomena encountered in the vicinity of the cutting edge, and to predict the thermo-mechanical loads applied on the tool and machined surfaces. It facilitates, for example, an improved tool design and machined surface integrity [1]. However, it is well known that the reliability of FE simulations depends largely on several interconnected factors; for example, implementation of appropriate frictional and thermal boundary conditions, and reliable material and damage models [2].

To this end, a vast number of studies have been dedicated to the derivation and development of representative material models and advanced methodologies for calibration of the constitutive parameters under the relevant range of strain, strain rate and temperature encountered in machining. These studies address two main different categories of constitutive models: (1) phenomenological models such as Johnson-Cook (JC) [2] and its modifications [3], and (2) the physics-based (dislocation-based) models [4]. The simplicity and availability of the phenomenological models (e.g., JC model) in the FE commercial codes such as ABAQUS, DEFORM 2D/3D and AdvantEdge have made them more popular. The physics-based models are, on the other hand, microstructure dependent in nature, and they can offer additional insights into the machined surface characteristics. For example, it is possible to simulate the evolution of dislocation density, hardness and grain size during machining. However, as stated by Malakizadi et al. [5], a major drawback of the dislocation-based models is perhaps the large number of input data needed for calibration. This has limited the application of these models for cutting simulation.

In this study, a physics-based constitutive model to simulate the flow stress behaviour of titanium alloy Ti6Al4V is proposed for cutting simulation. This model incorporates the effects of volume fraction and grain size of α-phase, the solid solution strengthening effects of the major substitutional alloying elements and the interstitial elements like O, N and C as well as dynamic recovery during strain evolution. The material model was calibrated using six SHPB test data at different strain rates and temperatures. This model is then coupled with a damage model to simulate the characteristic

2212-8271
10.1016/j.procir.2023.03.057

segmented chip formation that is commonly observed when machining Ti6Al4V. The parameters of the damage and friction model are obtained using an inverse approach, minimising the difference between the simulated and experimental cutting and feed forces as well as the chip morphology parameters. The details of the experimental procedures, material model and the modelling strategy are presented in this study and the credibility of the results are critically discussed. This article ends with an outlook for further developments.

2. Experimental procedure

2.1. Dynamic flow stress characterisation using SHPB

The experimental setup used for dynamic flow stress characterisation using the SHPB as well as the main properties of the test rig are shown in Fig. 1. The cylindrical specimen is positioned between the end faces of two tool-steel bars, into which a mechanical pulse is introduced with the use of a pneumatic pulse generator. After running through the incident bar, the pulse is partly reflected at the interface with the specimen and partly introduced into the specimen, which is subsequently compressed. On the opposite side of the sample, the impulse is again partly reflected and partly introduced into the transmission bar. The pulses are measured with the help of strain gauges in the middle of both bars and recorded with a HBM GEN3i-device. By evaluating the first reflected pulse in the incident bar and the first transmitted pulse in the transmission bar, the plastic deformation of the material can be characterised in the form of a stress-strain curve and a curve of the strain rate over time from which a representative mean value can be calculated. For a detailed description of the test principle, please refer to Zabel et al. [6]. The calculations of first-wave strain, stress, and strain rate were carried out using graphical analysis tool developed by Francis et al. [7].

Compared to the standard SHPB, the test setup has an essential enhancement: with the help of an induction heater, the material sample can be brought to an initial test temperature of up to 750 °C with a high heating rate in just a few seconds. This makes it possible to characterise the temperature influence and the interaction with the strain rate influence in a temperature interval that is very relevant for the chip formation zone.

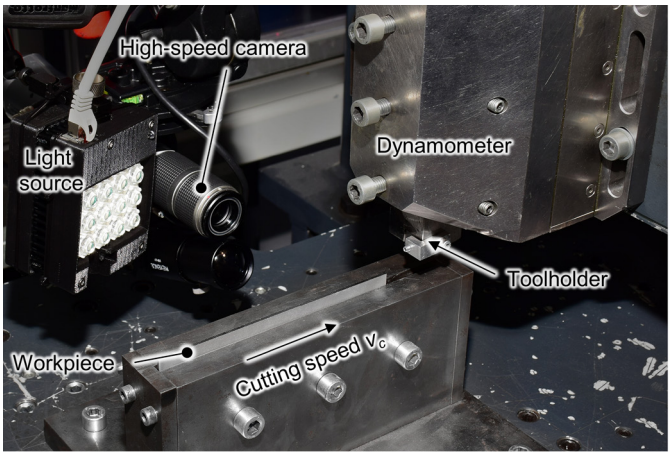

Fig. 2. The orthogonal cutting setup used in this study.

2.2. Orthogonal cutting experiments

For the inverse parameter identification as well as the validation of the simulation results, orthogonal cutting experiments have been conducted. For investigations on Ti6Al4V, a special machine tool from Heinz Berger Maschinenfabrik GmbH was used. The machine tool was specially designed for orthogonal cutting experiments. Cutting speed was varied at five steps between $v_c = 20$ m/min and 180 m/min while the uncut chip thickness was kept constant at $t_{uc} = 0.1$ mm. The width of cut w_c and the length of cut l_c were determined by workpiece geometry resulting in $w_c = 2$ mm and $l_c = 156$ mm. Cutting tools were simple wedges of uncoated submicron grain cemented carbide HF-K40. The orientation of cutting tool in tool holder results a rake angle of $\gamma = 0°$ and a clearance angle of $\alpha = 10°$. The cutting-edge radius was $r_\varepsilon = 10$ µm. In order to characterise the chip formation process, mechanical tool loads were measured with a piezoelectric dynamometer of type 9263 from Kistler AG, and chip morphology was recorded using optical microscope VHX5000 from Keyence GmbH. The experimental setup for orthogonal cutting is shown in Fig.2.

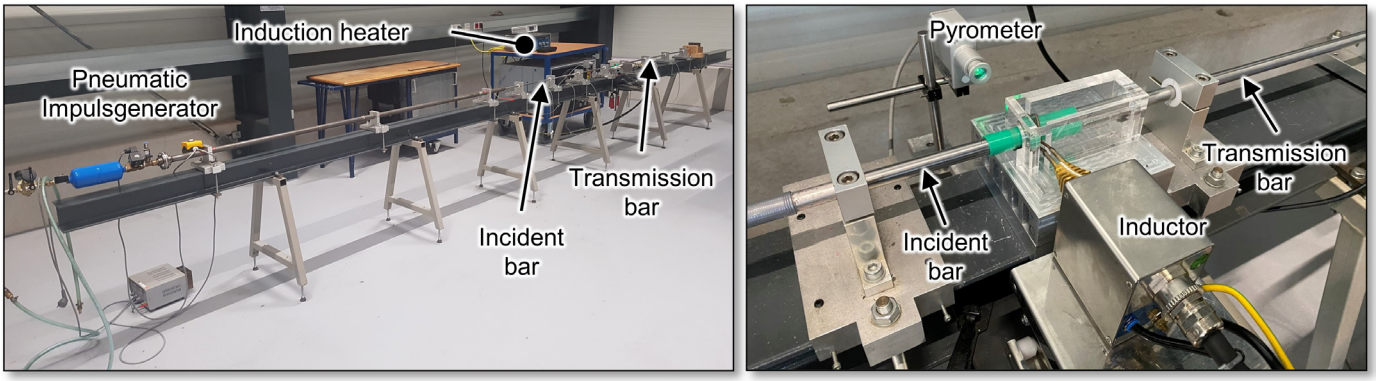

Bar material:	X37CrMoV5-1	Specimen length:	l_P = 4 mm
Bar length:	l_{bar} = 1500 mm	Specimen diameter:	d_P = 4 mm
Bar diameter:	d_{bar} = 14 mm	Data recorder:	HBM GEN3i
Projectile length:	l_{proj} = 400 mm	Sampling rate:	f = 1 MHz
Wave propagation speed:	c_s = 5231 m/s	Induction heater:	Himmelwerk HU2000Plus
		Max. Temperature:	T = 750 °C

Fig. 1. SHPB test rig used in this study indicting the setup for induction heating and the temperature measurement using pyrometer.

3. Material model

In a general sense, the tensile strength (flow stress properties) of metallic alloys can be described in a collective manner based on the underlying strengthening mechanisms [4, 8]. In case of Ti6Al4V, the flow stress properties may be expressed using the following relationship:

$$\sigma = \bar{\sigma} + \sigma_{HP} + \sigma_G \quad (1)$$

where $\bar{\sigma}$ accounts for the combined effects of lattice friction stress (Peierls-Nabarro stress) required to bypass the short-range obstacles and solid solution strengthening σ_{SS} for the mixture of α- and β-phases; σ_{HP} represents the Hall-Petch (grain boundary) effect and it is inversely proportional to the square root of average size α-Ti grains (i.e., $\sigma_{HP} = k_{HP}/\sqrt{D}$); σ_{SS} is the solid-solution strengthening effect; σ_G is the stress required for immobile dislocations to overcome long-range obstacles:

$$\sigma_G = \psi M \mu b \sqrt{\rho} \quad (2)$$

where ψ is a coefficient associated with interaction of dislocations in various slip systems (here $\psi = 0.3$), M is the Taylor factor, μ is the shear modulus, b is the Burgers vector of the dislocations, and the ρ represents the total density of immobile dislocations that evolves within the material during deformation. For a two-phase alloy like Ti6Al4V, $\bar{\sigma}$ can be described as:

$$\bar{\sigma} = (\sigma_0^{\alpha} + \sigma_{ss}^{\alpha})V_{\alpha} + (\sigma_0^{\beta} + \sigma_{ss}^{\beta})(1 - V_{\alpha}) \quad (3)$$

where σ_0^i and σ_{ss}^i represent the strengthening contributions associated with the lattice friction in absence of any alloying elements and solid solution effects for phase i, respectively, and V_{α} is the volume fraction of α-phase. Here, the volume fraction of α-Ti is adjusted at the elevated temperatures (T<1270K) by the following equation [9] :

$$V_{\alpha} = V_{\alpha}^0 \left(1 - \left(\frac{T}{1270}\right)^{10}\right) \quad (4)$$

where V_{α}^0 is the volume fraction of α-Ti in the microstructure at the room temperature. V_{α} is assumed to be zero at the temperature above 1270K. The lattice friction stress (σ_0^i) in Eq. 3 for the phase i can be expressed as [8]:

$$\sigma_0^i = \vartheta \mu_0^i \left(1 - \left[\frac{k_B T}{\varrho \mu_i b^3} ln\left(\frac{\dot{\varepsilon}_0}{\dot{\varepsilon}_p}\right)\right]^{1/p}\right)^{1/q} \quad (5)$$

where ϱ, p, q and ϑ are the Peierls–Nabarro stress constants; μ_0^i is the shear modulus of the parent phase i at 300 K; T is the temperature in Kelvin, μ_i is the shear modulus of the parent phase i at temperature T, k_B is the Boltzmann constant. The $\dot{\varepsilon}_p$ and $\dot{\varepsilon}_0$ are the equivalent strain rate induced by deformation and the reference strain rate, respectively. The temperature dependent shear modulus of a given (pure) metal may be estimated using the following relationship:

$$\mu_i = \mu_0^i \left(1 + \left(\frac{T - 300}{T_m}\right)\left(\frac{T_m}{\mu_0^i}\frac{d\mu_i}{dT}\right)\right) \quad (6)$$

T_m in this equation is the melting point in Kelvin. The solid solution strengthening terms (σ_{ss}^i) in Eq. 3 can be calculated by an extension of Labusch model [10] proposed by Toda-Caraballo and Rivera-Díaz-del-Castillo [11] for the multicomponent systems:

$$\sigma_{ss}^i = \left(\sum_j B_j^{3/2} x_j\right)^{2/3} ; B_j = ZM\mu\lambda_j^{4/3} \quad (7)$$

where x_j is the concentration of solute atom j (atomic fraction); Z is a constant, and λ_j represents the misfit caused by the solute atom j:

$$\lambda_j = \xi\left(\bar{\eta}_j^2 + \theta^2\delta_j^2\right)^{1/2} \quad (8)$$

ξ and θ are the constants associated with the crystallographic structure of the parent phase (number of active slip systems in α- and β-phases) and dominant dislocation type: screw or edge dislocations (here θ =16). $\bar{\eta}_j$ and δ_j are, respectively, the shear modulus and lattice parameter misfits inducted by the solute atom j. $\bar{\eta}_j$ may be approximated as [11]:

$$\bar{\eta}_j = \frac{\eta_j}{1+0.5|\eta_j|} ; \eta_j = \frac{2(\mu_j - \mu_i)}{(\mu_j + \mu_i)} \quad (9)$$

μ_j and μ_i in Eq. 9 is the temperature dependent shear modulus of the alloying element j and the parent phase i (α- and β-Ti allotropes), respectively. The lattice parameter misfit (δ_j) caused by the solute atom j can also be approximated by [11, 12]:

$$\delta_j = \frac{\gamma_i}{\gamma_j}\frac{(r_j - r_i)}{r_i} ; \gamma_i = 1 + \frac{4\mu_i}{3\kappa_i} ; \gamma_j = 1 + \frac{4\mu_i}{3\kappa_j} \quad (10)$$

where r_j and r_i are the atomic radius of the solute atom j and the parent phase i, while κ_j and κ_i are the bulk moduli of the substitutional alloying element j and the parent phase i, respectively. Eq. 6 is used to estimate the temperature dependent shear moduli, while the room temperature bulk moduli are used to calculate γ_i and γ_j in Eq. 10. The values of μ_0, T_m and $T_m\, d\mu/\, \mu_0\, dT$ in Eq. 6 are taken from Frost and Ashby [13] for the parent phase i (α- and β-Ti) and the major alloying (substitutional) element j in Ti6Al4V (i.e., Al, V and α-Fe). The solid solution strengthening contributions of the interstitial elements (O, N and C) in α-Ti are included by:

$$\sigma_{ss}^{\alpha} = \sum_i A_i x_i^{2/3} \quad (11)$$

Here, A_i (i=1, 2 and 3) is the solid solution strengthening constant representing the effects on O, N and C in α-Ti, and x_i is the concentration of solute atom i (atomic fraction of interstitial elements in α-Ti). Table 1 summarises the values of A_i estimated by the regression analysis based on the experimental data presented in [14].

To predict the flow stress evolution during material deformation, the rate with which the dislocations are generated and annihilated in the mixed alloy (with a given volume fraction of α- and β-phases and the grain size of α-phase) should be known. Here, Kocks-Mecking model [15] is used to estimate the change in the density of dislocations with strain:

$$\frac{d\rho}{d\varepsilon} = \frac{\Omega}{b}\sqrt{\rho} - \Lambda\rho \quad (12)$$

Ω and Λ in Eq. 12 are the parameters associated with the dislocation evolution and dynamic recovery, respectively. In this study, both parameters are assumed to be constant. Hence, the total density of dislocations can be calculated as a function

of strain, provided that Ω, Λ and the initial dislocation density (ρ_0) are known. Here, ρ_0 is assumed to be 5×10^{12} m^{-2}. Eq. 1 to 12 are implemented in a MATLAB code to obtain the flow stress of Ti6Al4V at a given temperature and strain rate.

Table 1. The model parameters taken from literature or obtained from the optimisation procedure. D and V_α^0 are the microstructural properties of the investigated alloy.

Parameter	α-Ti	β-Ti
k_{HP} $(MPa\sqrt{mm})$	7.3 [16]	–
D (mm)	0.008	–
V_α^0 $(-)$	0.85	0.15
M $(-)$	4.5 [17]	2.8 [18]
b (Å)	2.95 [13]	2.86 [13]
ϑ $(-)$	0.015 [13]	0.049*
ϱ $(-)$	0.14 [13]	1.73**
p $(-)$	1.33 [13]	1.3 [4]
q $(-)$	0.75 [13]	0.3 [4]
$\dot{\varepsilon}_0$ (s^{-1})	1e6 [13]	3.61e10 [4]
ξ $(-)$	1	4 [18]
Z $(-)$	0.015	0.0009 [18]
A_O (GPa)	8.517	–
A_N (GPa)	13.716	–
A_C (GPa)	2.985	–

* Calculated based on the value reported in [4].
** Calculated based on the value reported in [4] and the room temperature shear modulus of β-Ti.

Table 1 summarises the parameters estimated either by the model evaluation (minimisation problem) against SHPB test data at different temperature and strain rates or taken from the literature. The calibrated values of Ω and Λ are 0.29 and 43, respectively. Fig. 3 shows a comparison between the experimental SHPB results and the model predictions using the calibrated parameters.

4. Modelling procedure

For the cutting simulations in this investigation, the commercial software SFTC DEFORM 2D is used. The tool is included in the FE models as a rigid object; however, the heat transfer was allowed within the tool during the simulations. The element size in the tool is controlled using a mesh window, resulting in a fine element size (10 µm) near the cutting edge. The same method is used for the workpiece material to obtain a refined element size distribution in the vicinity of cutting edge and along the shear zones (resulting in a minimum element size of about 2.5 µm). The workpiece is assumed elasto-viscoplastic and the Lagrangian incremental FE formulation is used for the cutting simulations. The elastic and thermal properties of Ti6Al4V are taken from DEFORM database (Ti6Al4V-machiningSFTC), while the viscoplastic behaviour of the material is modelled using Eq. 1.

A modified Cockcroft-Latham (CL) fracture criterion is used here to estimate the damage onset:

$$W_{CL} = \int \sigma^* \dot{\varepsilon}_p dt \; ; \; \sigma^* = \begin{cases} \sigma^* = \sigma_e & \sigma_1 > 0 \\ \sigma^* = 0 & \sigma_1 < 0 \end{cases} \quad (13)$$

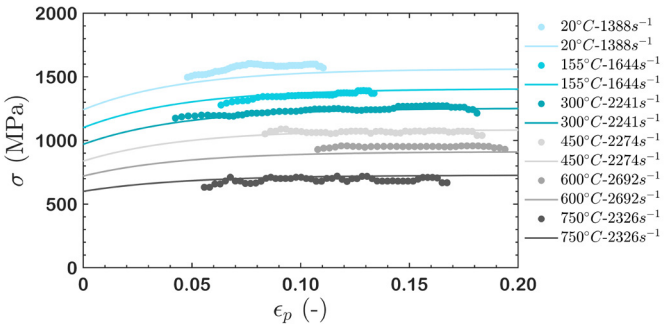

Fig. 3. Experimental and simulated flow stress behaviour of Ti6Al4V at various temperatures and strain rates.

In Eq. 13, σ_e and σ_1 represent the equivalent von Mises and first principal stresses, respectively. Eq. 13 is implemented using a Fortran subroutine in DEFORM 2D. For each element, as soon as W_{CL} during the chip formation process exceeds a predefined value, the flow stress instantaneously scales down by the factor δ. This allows to simulate the crack formation phenomenon when machining Ti6Al4V.

In this study, a pressure dependent shear friction model is implemented using a Fortran subroutine to simulate the frictional condition at the tool-chip interface:

$$\tau_f = [1 - \exp(-\alpha_1 \sigma_n)]k \quad (14)$$

τ_f and σ_n in Eq. 14 are the shear and the normal stresses acting on the tool surfaces and k is the shear strength of workpiece material estimated by Eq. 1 ($k = \sigma/\sqrt{3}$), and α_1 is a constant. A perfect thermal condition was assumed between the tool, chip and workpiece materials. This was achieved by defining a large heat transfer coefficient of $h = 10^5$ kW/m^2°C. The viability of the assumed thermal and frictional boundary conditions is discussed in detail in previous studies [19]. Table 2 summarises the damage and friction model parameters obtained by evaluation of the cutting and feed forces as well as the chip morphology parameters (i.e., the maximum and minimum chip thicknesses) at v_c = 20 m/min.

Table 2. The parameters of the damage and friction models.

W_{CL} (MPa)	δ	α_1
200	0.4	0.0045

A MATLAB code is developed to create the flow stress data in the tabulated format consistent with DEFORM 2D assumptions. The flow stress curves for Ti6Al4V at different ranges of strain (up to 5), strain rate (up to 10^5 s^{-1}) and temperature (up to 1200K) are calculated using the MATLAB code and the then written in the KEY files.

5. Results and discussion

The FE simulation results at different cutting speeds are shown in Fig. 4. As evident, the FE models are able to predict the segmented chip formation when machining Ti6Al4V under the attempted cutting conditions. The maximum and minimum chip thicknesses decrease with the cutting speed and the cracks propagate deeper, as also experimentally observed during the

cutting tests (see Fig. 5 (a)). However, the deviation with the experimental results increases at higher cutting speeds. As shown in Fig. 5 (b), the FE simulations underestimate the maximum chip thickness values, while they overestimate the minimum chip thicknesses. The cutting and feed forces, as shown in Fig. 5 (c), are also underestimated in all cases, although the underestimations in the simulated feed forces are more pronounced. The cutting forces are underestimated between 2-14 %, the lowest and highest deviations are associated with $v_c = 20$ m/min and $v_c = 140$ m/min, respectively. In case of feed force, the simulation errors span between 8-37 %. Here, the lowest and largest deviations from the experimental feed force measurements are observed at $v_c = 20$ m/min and the highest $v_c = 180$ m/min. Overall, this range of simulation error is deemed reasonable as compared to the previous attempts reported in the literature using modified Johnson-Cook (JC) constitutive models; see for example the studies performed by Calamaz et al. [20] and Sima and Özel [3]. The maximum interface temperatures also seem reasonable [3], varying between 470°C at $v_c = 20$ m/min to 880°C at $v_c = 180$ m/min.

Fig. 6 shows the distribution of the dislocation density estimated using the calibrated Kocks-Mecking dislocation evolution model at $v_c = 60$ m/min. The results coincide well the distribution of effective strain shown in Fig. 4. The highest dislocation densities occur near the tool-chip interface on the secondary shear zone, on the machined surface and within the shear localised regions of the segmented chip. However, as evident, the dislocation density is rapidly saturated at high strain regions in the chip. This behaviour is observed because a large dynamic recovery constant (Λ) is used in Eq. 12 to match the SHPB test data at the applicable ranges of strains above $\varepsilon = 0.05$, resulting in a rapid dynamic recovery (dislocation density saturation) at strains as low as $\varepsilon = 0.02$. This small strain threshold results in a fast dislocation density saturation in the shear zones. Therefore, no significant strain hardening effect is expected above this strain threshold, as shown in Fig. 3. This can partly be the reason for the simulation errors in Fig. 5.

Nevertheless, the physics-based (i.e., dislocation-based) constitutive model presented in this study enables a microstructure dependent derivation of the material

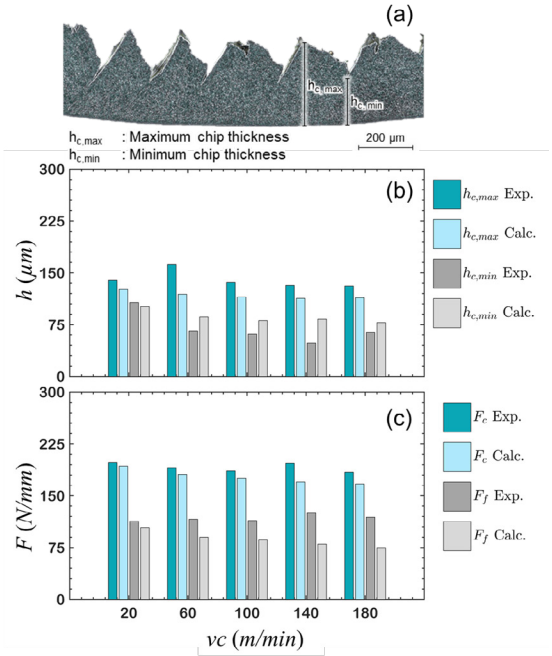

Fig. 5: (a) Serrated chip formation and its parameters: $h_{c,max}$ and $h_{c,min}$; (b) simulated and experimental chip thickness parameters; (c) simulated and experimental cutting and feed forces (F_c and F_f), $t_{uc} = 0.1$ mm.

viscoplastic properties required for machining simulations. For example, the presented model can provide the flow stress properties of the Ti6Al4V as the volume fraction and the average grain size of α-Ti change due to an arbitrary thermal treatments (provided that the heat treatment does not result in Widmanstätten microstructure, since the effect of acicular α- and α'-Ti is not included here), or when the concentration of interstitial elements like O, N and C varies in the workpiece material. Hence, the presented physics-based model reduces the needs for costly experimental tests for a new batch of material with different chemical composition and microstructural properties. Yet the capabilities of the current physics-based model for the cutting simulation can be improved further, for example, by including a temperature dependent dislocation-drag stress contribution as proposed in [4, 13]. The dislocation-drag stress accounts for the marked hardening effects experimentally observed at very high strain rates. The neglection of this effect is perhaps another reason for

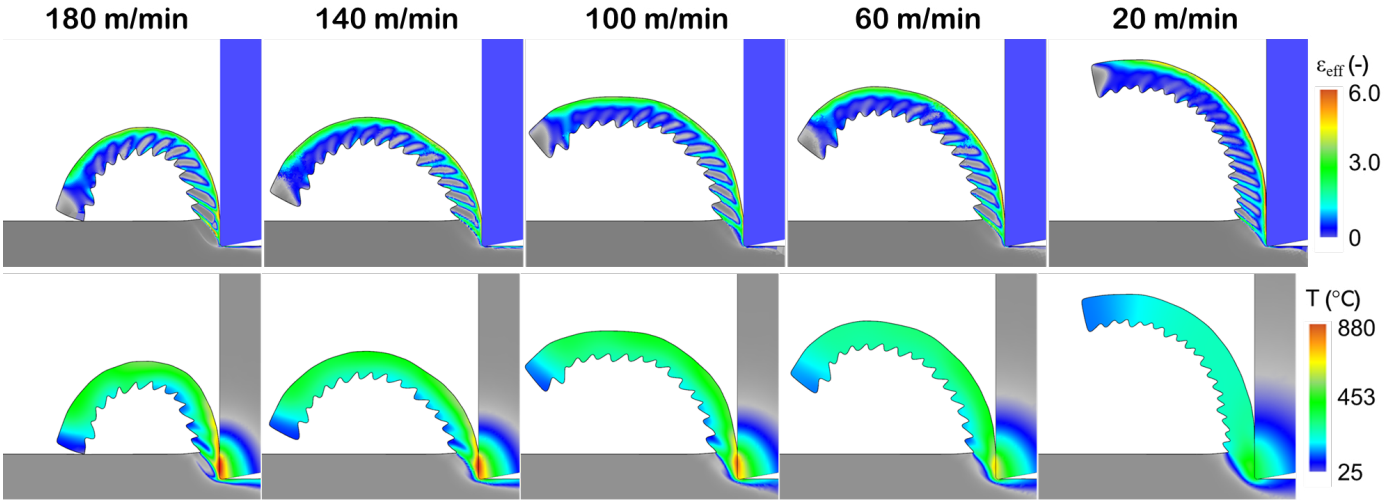

Fig. 4. The FE simulation results (temperature and effective strain) at different cutting speeds varying between $v_c = 20$ - 180 m/min. $t_{uc} = 0.1$ mm.

the underestimation of the cutting forces in this study, despite the reasonable match between the model estimations and SHPB test data (see Fig. 3). Nevertheless, a more advanced calibration strategy (see for example [5]) is to be implemented to determine the dislocation-drag stress contribution at a wide range of temperature and strain rate encountered in cutting. In addition, the application of more advanced dislocation evolution models [8], and the adoption of the physics-based (progressive) damage models [21, 22] can enhance the model predictions. These topics will be addressed in our future investigations.

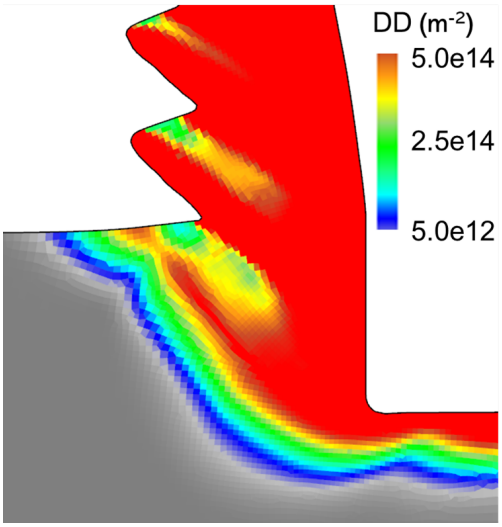

Fig. 6. The distribution of the total dislocation density simulated using Eq. 12 and the parameters given in Table 1: v_c = 60 m/min, t_{uc} = 0.1 mm.

6. Conclusions

This study presents a robust physics-based microstructure sensitive flow stress model for Ti6Al4V. The results of the cutting simulations with the calibrated material and damage model indicated the significant potential of this approach compared to the phenomenological constitutive models such as the commonly used Johnson-Cook model. Calibrated using only six SHPB tests, this model can predict the forces and chip morphology parameters with acceptable error margins. The reliability of the FE simulation results can be improved further by including dislocation-drag stress contribution and implementation of a more advanced damage model.

Acknowledgements

Funded by the Deutsche Forschungsgemeinschaft (DFG, German Research Foundation). Gefördert durch die Deutsche Forschungsgemeinschaft (DFG) – Projektnummer 421463266. Amir Malakizadi would also like to acknowledge the financial support of the Chalmers Area of Advance – Production and the support received from Chalmers Centre for Metal Cutting Research (MCR). Part of this research is financed by Swedish national research program Vinnova-FFI (2020-05179).

References

[1] P. J. Arrazola, T. Özel, D. Umbrello, M. Davies, and I. S. Jawahir, "Recent advances in modelling of metal machining processes," CIRP Annals - Manufacturing Technology, vol. 62, no. 2, pp. 695-718, 2013.
[2] S. N. Melkote et al., Advances in material and friction data for modelling of metal machining, CIRP Annals, vol. 66, no. 2, pp. 731-754, 2017.
[3] M. Sima and T. Özel, Modified material constitutive models for serrated chip formation simulations and experimental validation in machining of titanium alloy Ti–6Al–4V, International Journal of Machine Tools and Manufacture, vol. 50, no. 11, pp. 943-960, 2010.
[4] P. Fernandez-Zelaia, S. Melkote, T. Marusich, and S. Usui, A microstructure sensitive grain boundary sliding and slip based constitutive model for machining of Ti-6Al-4V, Mechanics of Materials, vol. 109, pp. 67-81, 2017.
[5] A. Malakizadi, J. N. Oberbeck, M. Magnevall, and P. Krajnik, A new constitutive model for cutting simulation of 316L austenitic stainless steel, Procedia CIRP, vol. 82, pp. 53-58, 2019.
[6] A. Zabel, T. Rödder, and M. Tiffe, Material testing and chip formation simulation for different heat treated workpieces of 51CrV4 steel, Procedia CIRP, vol. 58, pp. 181-186, 2017.
[7] D. K. Francis, W. R. Whittington, W. B. Lawrimore, P. G. Allison, S. A. Turnage, and J. J. Bhattacharyya, "Split Hopkinson Pressure Bar Graphical Analysis Tool," Experimental Mechanics, vol. 57, no. 1, pp. 179-183, 2017.
[8] B. Babu and L.-E. Lindgren, "Dislocation density based model for plastic deformation and globularization of Ti-6Al-4V," International Journal of Plasticity, vol. 50, pp. 94-108, 2013.
[9] R. C. Picu and A. Majorell, "Mechanical behavior of Ti–6Al–4V at high and moderate temperatures—Part II: constitutive modeling," Materials Science and Engineering: A, vol. 326, no. 2, pp. 306-316, 2002.
[10] R. Labusch, "A Statistical Theory of Solid Solution Hardening," physica status solidi (b), vol. 41, no. 2, pp. 659-669, 1970.
[11] I. Toda-Caraballo and P. E. J. Rivera-Díaz-del-Castillo, "Modelling solid solution hardening in high entropy alloys," Acta Materialia, vol. 85, pp. 14-23, 2015.
[12] V. A. Lubarda, "On the effective lattice parameter of binary alloys," Mechanics of Materials, vol. 35, no. 1, pp. 53-68, 2003.
[13] H. J. Frost and M. F. Ashby, "Deformation-mechanism maps for metals and alloys," 1981.
[14] E. W. Collings and H. L. Gegel, "Physical Principles of Solid Solution Strengthening in Alloys," in Physics of Solid Solution Strengthening, E. W. Collings and H. L. Gegel Eds. Boston, MA: Springer New York, 1975, pp. 147-182.
[15] U. F. Kocks and H. Mecking, "Physics and phenomenology of strain hardening: the FCC case," Progress in Materials Science, vol. 48, no. 3, pp. 171-273, 2003.
[16] Y. Chong, G. Deng, S. Gao, J. Yi, A. Shibata, and N. Tsuji, "Yielding nature and Hall-Petch relationships in Ti-6Al-4V alloy with fully equiaxed and bimodal microstructures," Scripta Materialia, vol. 172, pp. 77-82, 2019.
[17] H. E. Friedrich and B. L. Mordike, Magnesium technology. Springer, 2006.
[18] G. H. Zhao, X. Z. Liang, B. Kim, and P. E. J. Rivera-Díaz-del-Castillo, "Modelling strengthening mechanisms in beta-type Ti alloys," Materials Science and Engineering: A, vol. 756, pp. 156-160, 2019.
[19] A. Malakizadi, K. Hosseinkhani, E. Mariano, E. Ng, A. Del Prete, and L. Nyborg, Influence of friction models on FE simulation results of orthogonal cutting process, The International Journal of Advanced Manufacturing Technology, journal article vol. 88, no. 9, pp. 3217-3232, 2017.
[20] M. Calamaz, D. Coupard, and F. Girot, A new material model for 2D numerical simulation of serrated chip formation when machining titanium alloy Ti–6Al–4V, International Journal of Machine Tools and Manufacture, vol. 48, no. 3, pp. 275-288, 2008.
[21] S. Razanica, A. Malakizadi, R. Larsson, S. Cedergren, and B. L. Josefson, FE modeling and simulation of machining Alloy 718 based on ductile continuum damage, International Journal of Mechanical Sciences, vol. 171, p. 105375, 2020.
[22] W. Cheng, J. Outeiro, J.-P. Costes, R. M'Saoubi, H. Karaouni, and V. Astakhov, A constitutive model for Ti6Al4V considering the state of stress and strain rate effects, Mechanics of Materials, vol. 137, p. 103103, 2019.